Experimental and numerical structural analysis of a windsurf fin

F. Nascimento, L.S. Sutherland & Y. Garbatov
Centre for Marine Technology and Engineering (CENTEC), Instituto Superior Técnico,
Technical University of Lisbon, Portugal

Abstract: Structural analyses, both numerical and experimental, have been made of a composite windsurf fin. Structural analyses, both numerical and experimental, have been made of a composite windsurf fin. An FE model was developed employing commercial software ANSYS using both linear and nonlinear analyses of the structural response due to external loads (selected to give an approximation of the in-service longitudinal deformation) giving the resulting stresses and deflections. To calibrate and validate the numerical model, experimental tests using a servo-hydraulic mechanical test machine were performed. To try to estimate the failure load of the fin Tsai-Wu, Maximum Stress and Maximum Strain failure criteria were applied.

Key-Words— ANSYS, Composite Materials, Finite Element Method, Tsai-Wu, Ultimate Strength

1. INTRODUCTION

Fibre reinforced plastic (FRP) composite materials are now ubiquitous in the marine industry, offering many advantages over the use of steel, aluminium or wood, such as resistance to corrosion and rot, ease of forming complex seamless shapes, and high specific material properties. due to such advantages (Sutherland, 2018). For cases with a highly loaded structure that also requires thinner sections due to hydrodynamic considerations such as windsurfer fins (or hydrofoils) composites are often the only feasible solution. Since these fins must be both thin for efficient hydrodynamic performance and strong enough not to break under the often very demanding loadings asked of them it is important to be able to predict their structural response.

There is little previous work concerning windsurfer fins, although there were a few scientific studies on windsurfer fin performance, mostly as the sport increased rapidly in popularity in the 1990's (Broers et al., 1992, Sutherland, 1993, Sutherland & Wilson, 1994, Kunoth et al., 2007, Gourlay & Martellotta, 2011) and there are various articles of varying technical depth in the windsurfing press and online, e.g. (Fagg, 1997, Drake, 2005)[.

The complex nature of both composite materials and the internal structural arrangement of a fin mean that a correspondingly complex numerical analysis such as FEM is required to analyse structural responses. Also, very small changes in deflections can result in important consequences in terms of hydrodynamic efficiency and control, especially in a competitive environment. The fins studied here are fabricated by F-Hot Fins and are used by top international sailors and even world champions. Hence the scope for obtaining a structural model that will be developed to allow faster and easier evaluation of future improvements to the foil sections, planforms and lay-ups of these fins is of great interest.

Hence, the aim here is to develop an initial FE model of an actual windsurfer fin and to both calibrate and validate the model in terms of stiffness and deflection responses with full-scale mechanical tests on the fabricated fin itself. Finally, Letters f, m and c are used to indicate fibre, matrix and composite respectively. Volume and weight fractions are denoted by V and W respectively estimates of the ultimate strength of the fin will be made using various failure criteria. The FE model obtained will be the first stage in an overall work incorporating parallel computational fluid dynamics (CFD) and fluid structure interaction (FSI) studies to obtain a design tool for the improvement of windsurfer fin design, or in fact for other underwater foils.

2. MATERIAL PROPERTIES

The material property inputs to an FE model are essential in ensuring that correct results are obtained, but this is often the most difficult part of this type of numerical modelling due to the large number of properties required for these anisotropic materials. Further, this is usually even more challenging since the composites used in the marine industry are hand produced, as they are in this case, leading not only to inherent variability, but also to very non-standardised materials (Sutherland, 2018).

One of the most basic properties which will both depend on the exact production method and conditions (and even laminator) considered and affect many of the strength and especially stiffness material properties is the relative proportions of fibre and matrix, expressed as either weight or volume fractions. For theoretical analysis, volume fractions are more helpful but weight fractions are easier to obtain experimentally, but they are easily converted knowing the raw fibre and matrix densities (Shenoi & Wellicome, 1993).

Fibre weight fraction (FWF) is easily measured from mass measurements taken during fabrication:

$$FWF = \frac{m_f}{m_f + m_m} \quad (1)$$

where the subscripts *f* and *m* refer to fibre and matrix, respectively

And this is then converted to fibre volume fraction (FVF) via

$$FVF = \frac{1}{\left[1 + \frac{\rho_f}{\rho_m}\left(\frac{1}{FWF} - 1\right)\right]} \quad (2)$$

where ρ is density.

The thickness of each ply is also of great importance in developing the geometrical model, and this is given by Shenoi and Wellicome (1993):

$$t = \frac{W_F}{\rho_f . FVF . 1000}\ [mm] \quad (3)$$

where W_F is the 'fibre areal weight' in g/m^2

The exact amounts of materials used were measured by Steve Cook at F-hot fins and Eqn (1) presented an average FWF of about 0.41. The densities of the epoxy resin, and the E-glass and carbon reinforcements were 1.2, 2.6 and 1.5 g/cm^3 respectively (AG, 2000, Exel, 2016), applying Eqn (2) the FVF values are estimated approximately as 0.3 and 0.4 for E-glass and carbon plies, respectively.

Based on Eqn (3) the ply thicknesses are estimated as:

- 100 g/m^2 woven carbon 0.17 mm
- 200 g/m^2 woven carbon 0.34 mm
- 100 g/m^2 unidirectional carbon 0.17 mm
- 200 g/m^2 unidirectional E-glass 0.28 mm

Knowing the fibre and matrix materials, the approximate FVF values and the production process used, initial estimates of mechanical properties from the test data reported in (Miller, 1991) and the ANSYS materials property library were defined as can be seen in Table 1.

Table 1. Initial Stiffness Values

	Units	Epoxy Carbon UD	Epoxy Carbon Woven	Epoxy E-Glass UD
E_x	MPa	121000	61340	45000
E_y	MPa	8600	61340	10000
E_z	MPa	8600	6900	10000

3. FINITE ELEMENT MODEL

A finite element model is created using the commercial software ANSYS (2009). The model consists of 2597 nodes and 2610 elements. Most of the generated finite elements are quadrilateral, of a size from 2 to 10 millimetres. Shell element, type SHELL181, is used. This element is a four-node finite element with six degrees of freedom at each node, including translations and rotations in the x, y, and z axes. SHELL181 element is well-suited for linear and nonlinear large deflection finite element analyses (see Figure 1).

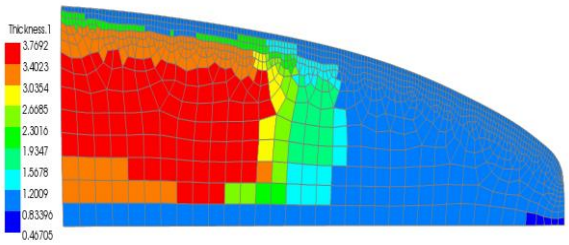

Figure 1- Finite element thickness

Figure 1 shows a thickness distribution over the fin. The root of the fin, located in the fixed support, is thicker and hence has more plies and it is the most highly stressed area.

The lay-up includes woven and unidirectional carbon and E-glass reinforcements, as can be seen in Figure 2. The fin is symmetrical about the centre line and Figure 2 only shows the half of the fin and the ply identification numbers used. The two identical halves of the fin were identified as 'TOP' and 'DOWN' referring to their positions in the mechanical tests.

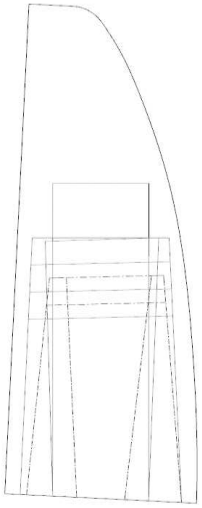

Figure 2- Lay-up plan

The boundary conditions of the finite element model are shown in Figure 3, fully representing the set-up of the experimental test.

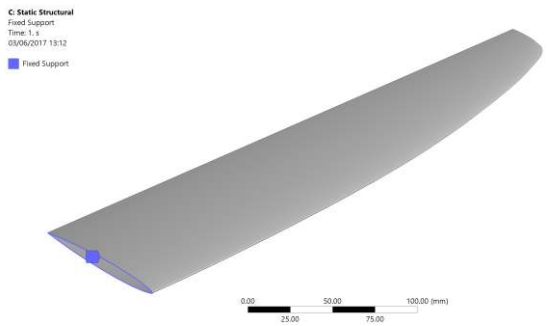

Figure 3- Boundary conditions

4. MECHANICAL TESTS

A calibrated computer-controlled servo-hydraulic machine was used to perform the mechanical tests, recording force and displacement with time. In terms of supports, it was a simple matter to clamp the fin base to avoid any rotation or translations (see Figure 4) as would be the case in-service. However, it was not feasible to replicate the varying distributed hydrodynamic loading that the fin would be subjected to in the water and hence a simple point load, applied via a 10 mm diameter hemispherical steel load applicator was used (see Figure 4).

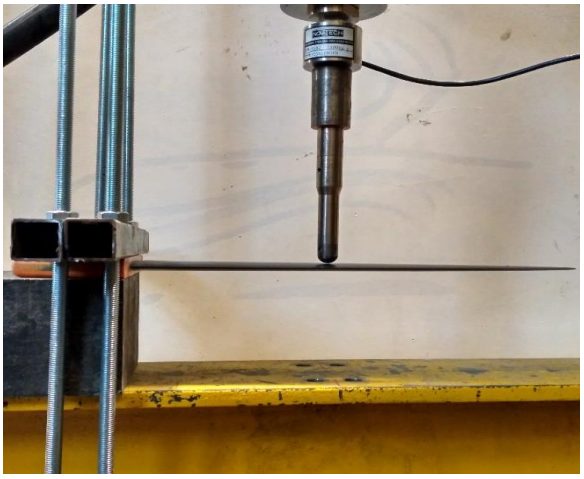

Figure 4. Experimental Set-up

The application point of the point load was, however, selected to give the best approximation of the in-service loading. The load was applied at the quarter chord distance from the leading edge, corresponding to the effective position of the hydrodynamic loading. Also, the centre of pressure of a semi-elliptic loading is at approximately 40% span, and so the fin was loaded at this point (see Figure 5).

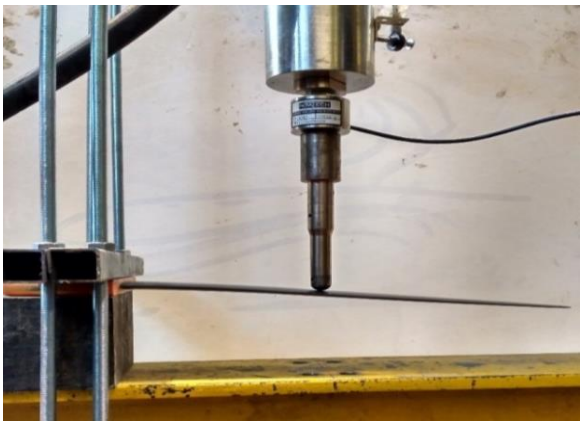

Figure 5- 40% Span Test

Further, since the in-service loading is distributed, applying the load at twice this distance gives a reasonable approximation to the working lengthwise-deformed shape, and hence the fin was also tested with the load at 80% span (see Figure 6).

Loading was applied under displacement control at a speed of 0.1 mm/s up to approximately 40% of the estimated failure load to ensure that the fin was not damaged as it would be needed for later mechanical and hydrodynamic testing; the main objectives of these tests was to calibrate the material property inputs to the FE model.

The resultant force-deflection results from both tests are shown in Figure 7 and Figure 8. The 'Unfiltered data' is the raw data from the sensors, but the very high R2 values of the fitted lines show that once electrical and other noise has been removed, the mechanical behaviour is very linear. This indicates that, up to the loadings used in these tests, no significant damage had occurred.

Figure 6. 80% span test

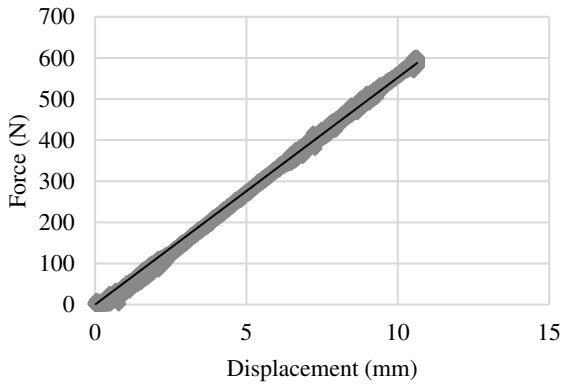

Figure 7- Force-Displacement, 40% span

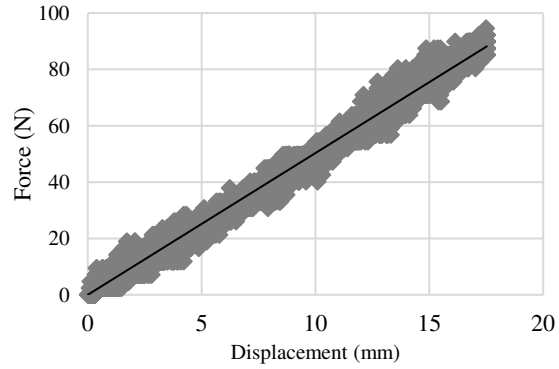

Figure 8 - Force-Displacement, 80% span

5. FEA MODEL CALIBRATION

To validate the developed finite element model, an idealized scenario is assumed, where, the report of Miller (1991), related to the mechanical properties of tested fin, is used to perform an initial estimation of the force-displacement relationship and the final calibration of the mechanical properties is performed using the result of the experimental tests.

The force-displacement relationship of the initial numerical estimate and experimental ones are shown in Figure 9. The first estimation of the force-displacement relationship, in the case of 40% of span, shows that the first assumption about the mechanical properties leads to an overestimation of the strength.

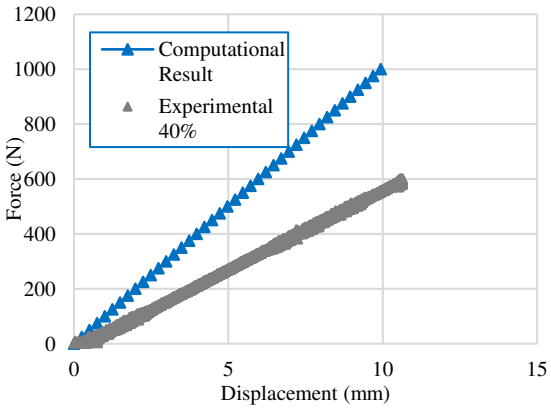

Figure 9- Force- displacement relationship, 40% span

To adjust the numerical model to the experimental results the Young moduli were calibrated, and the final values are presented in Table 1 and the resulting force-displacement relationship in Figure 10.

Table 1 - Young moduli of fibers

	Units	Epoxy Carbon UD	Epoxy Carbon Woven	Epoxy E-Glass UD
E_x	MPa	58606	30670	12000
E_y	MPa	2413	30670	2668
E_z	MPa	2413	3450	2668

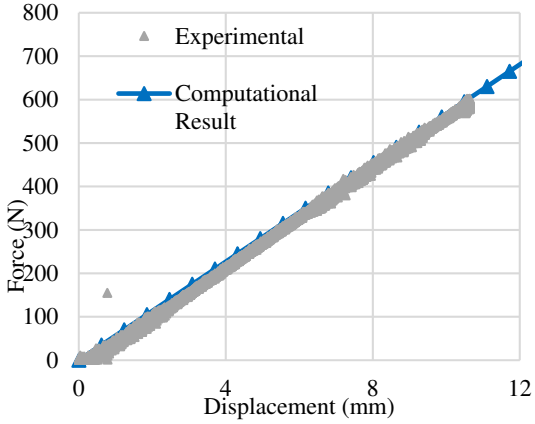

Figure 10 - Force-displacement, 40% span

The moment-curvature, M=(k) is presented in Figure 11, demonstrating a strong linear relationship between the moment and curvature.

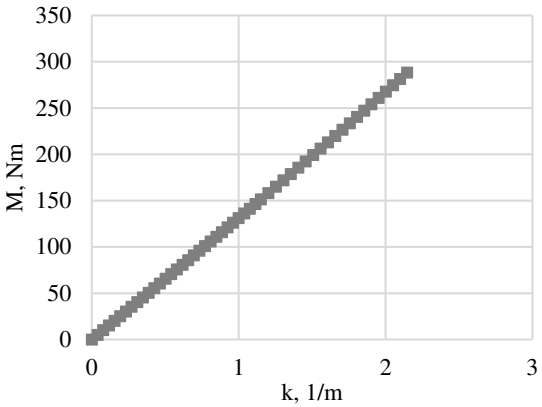

Figure 11- Moment- curvature relationship

In terms of displacement, when the fin is subjected to a concentrated force of 1,000 N, the fin behaviour is shown in Figure 12, where the deformed and undeformed shapes of the fin can be seen.

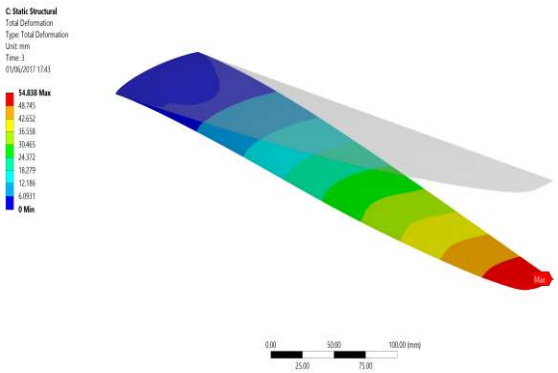

Figure 12 - Displacement (z), 1,000N

The distribution of the first principal stresses as a result of the loading force of 1,000 N is shown in Figure 13, where can be seen that the maximum stresses are located closely to the clamped support area.

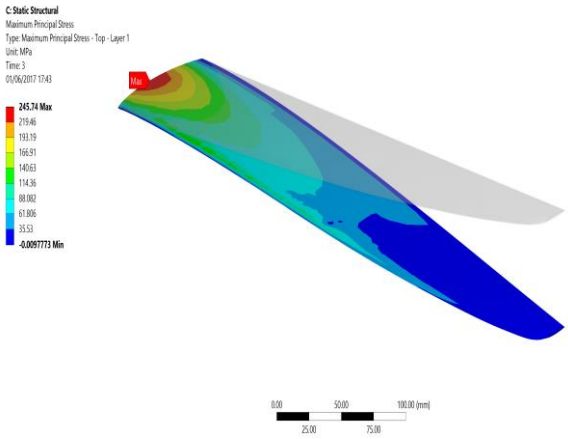

Figure 13 First principal stresses, 1,000 N

The distribution of shear stresses, when applying a concentrated force of 1,000 N is presented in Figure 14.

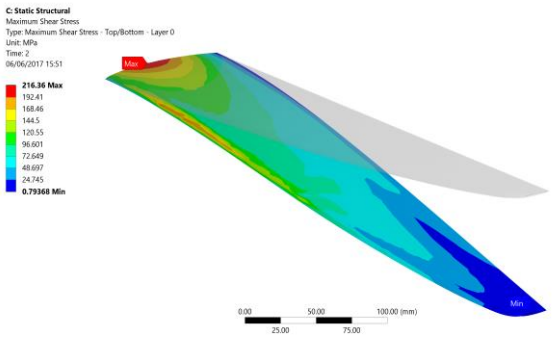

Figure 14 - Shear stresses, 1,000 N

6. FAILURE ANALYSIS

The critical failure load is estimated by using the Tsai and Wu (1971) failure criterion. Unlike the conventional isotropic materials, where one critical stress constant will suffice for the failure assessment, the composite materials require more elaborate methods to establish a failure criterion. The strength of the composite can be defined based on the strength of the individual plies. In addition, the failure of the plies occurs consequently as the applied load increases. It means that there may be a sequence of the first ply failure followed by other ply failures until the last one fails, denoting the ultimate failure. The progressive failure is therefore a quite complex in composite structures

The Tsai- Wu failure criterion is used here to identify the failure based on the stresses and material properties. A failure index of 1 denotes the onset of failure, and a value less than 1 denotes no failure. The Tsai-Wu failure criterion is commonly used for orthotropic materials with unequal tensile and compressive strengths. The failure index is defined as:

$$\text{F.I.} = F_1\sigma_1 + F_2\sigma_2 + F_{11}\sigma_1^2 + F_{22}\sigma_2^2 + F_{33}\tau_{12}^2 + 2F_{12}\sigma_1\sigma_2 \quad (4)$$

where

$$F_1 = \frac{1}{X_t} - \frac{1}{X_c}\ ;\ F_2 = \frac{1}{Y_t} - \frac{1}{Y_c};\ F_{11} = \frac{1}{X_t X_c}; \quad (5)$$

$$F_{22} = \frac{1}{Y_t Y_c};\ F_{33} = \frac{1}{{\tau_{12}}^2}; F_{12} = \frac{-1}{2\sqrt{Y_t Y_c X_t X_c}} \quad (6)$$

where the coefficient F_{12} represents the interaction between σ_1 and σ_2, and X_c, Y_c are the compressive strength and X_t, Y_t are the tensile strength of the material in the longitudinal (X) and transversal direction (Y). The parameter τ_{12} is the in-plane shear strength of the material.

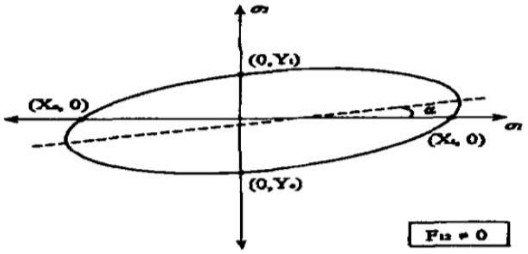

Figure 15- Tsai-Wu failure surface

A sample of the resulting Tsai-Wu failure surface is shown in Figure 15:

Applying the Tsai-Wu criterion, the critical load that produces the first ply failure is identified as 910N in the case when the 1st ply is under compression as can be seen in Figure 16.

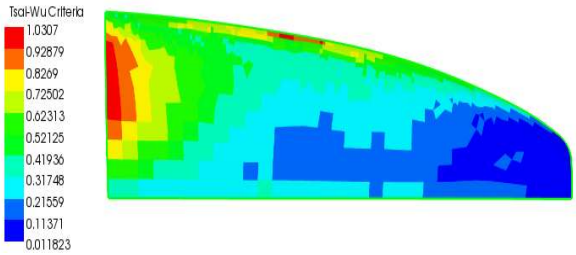

Figure 16 - Tsai-Wu failure

Higher stress values are concentrated near the clamped support (the left hand side of the fin in Figure 16). It is also observed some higher stresses in a small region near the leading edge around the half of the span, which may be developed because of the denser finite element mesh.

Although, the Tsai-Wu criterion identifies the presence of failure, it does not specify the type of failure. Two additional criteria for verifying the stress-strain behaviour of the fin with respect to the maximum stress and strain are applied here, considering three different failure conditions (Camanho et al., 2015):

$$Fibre:\ \sigma_1 \geq \sigma_{1T}^u \ \ or\ \ |\sigma_1| \geq \sigma_{1C}^u \quad (7)$$

$$Matrix:\ \sigma_2 \geq \sigma_{2T}^u \ \ or\ \ |\sigma_2| \geq \sigma_{2C}^u \quad (8)$$

$$Shear:\ |\sigma_{12}| \geq \sigma_{12}^u \quad (9)$$

Verifying the fibre failure, the required force to achieve this failure mode has to be above 2,050 N, and the area near the clamped support firstly demonstrate this failure mode, which is associated with the compressed part of the fin related to 4.DOWN ply.

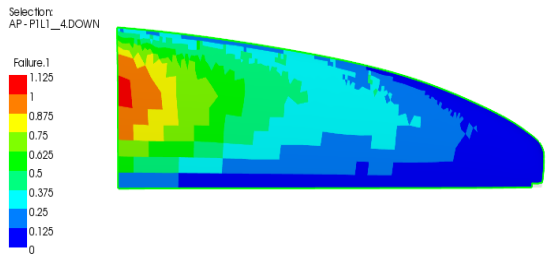

Figure 17 - Fibre failure- maximum stress

Three different failure conditions are considered in respect to the maximum strain of fibre direction, matrix or transversal direction and for shear strains:

$$Fibre:\ \varepsilon_1 \geq \varepsilon_{1T}^u \ \ or\ \ |\varepsilon_1| \geq \varepsilon_{1C}^u \quad (10)$$

$$Matrix:\ \varepsilon_2 \geq \varepsilon_{2T}^u \ \ or\ \ |\varepsilon_2| \geq \varepsilon_{2C}^u \quad (11)$$

$$Shear: \ |\sigma_{12}| \geq \sigma_{12}^{u} \quad (12)$$

Figure 18 shows the failure with respect to the maximum strain that occurs in the compressive side, ply 4.DOWN, when the loading force reaches a value of 825 N. The failure verifications are shown in Table 2.

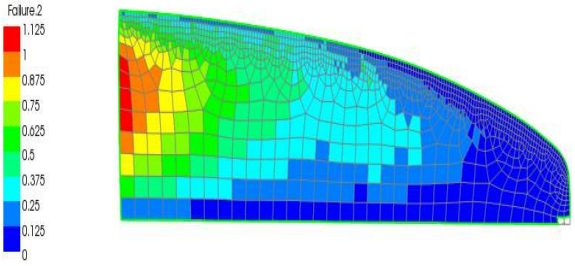

Figure 18- Fibre failure- maximum strain

Table 2- Failure criteria

Failure Criterion	Force (N)	Ply Failure	Deflection (mm)	Stresses (MPa)
Tsai-Wu	910	1.DOWN	49.902	223.62
Max Stress	2050	4.DOWN	109.68	393.18
Max Strain	825	4.DOWN	40.031	201.51

Table 2 also shows that the first failure criterion is in a very close agreement with the one of the maximum strain, indicating that the fibres stretch more. The Tsai-Wu failure criterion indicates a relatively low force of failure, which is associated with the matrix. All criteria show failure in plies that are subjected to compressive loading.

7. CONCLUSIONS

An initial FE model of a production windsurfer fin has been developed, calibrated and validated experimentally in terms of stiffness and deflection responses with full-scale mechanical tests.

The tracking down of relevant material property input data was a problem, but suitable initial values were found and then calibration of these values with the force-deflection data from the mechanical tests enabled a good fit of the predicted numerical results with the actual experimental behaviour.

The FE model gave a highly linear behaviour, with only a very short 'pseudo-plastic' due to failure mechanisms just before final failure. Initial failure load estimations have been made using the Tsai-Wu, Maximum Stress and Maximum Strain criteria, but further work should include experimental testing of the fin to failure to verify these values.

The current FE model will now be developed to allow exploration and optimisation of the laminate lay-up schedule and will be combined with a parallel computational fluid dynamics (CFD) work to finally give a working fluid structure interaction (FSI) model.

8. REFERENCES

AG, G. H. 2000. Guide to Composites.

ANSYS 2009. Online Manuals, Release 12.

Broers, A. M., Chiu, T. W., Pourzanjani, M. M. A., Buckingham, B. J. & van den Bersselaar, T. 1992. The Effects of Tip Flexibility on the Performance of a Blade-Type Windsurfer Fin. *Manouevring and Control of Marine Craft.* Comput. Mech. Publ, 261–273.

Camanho, P. P., Arteiro, A., Melro, A. R., Catalanotti, G. & Vogler, M. 2015. Three-dimensional invariant-based failure criteria for fibre-reinforced composites. *Int. J. Solids Struct.,* 55**,** 92-107.

Drake, J. 2005. *An Introduction to the Physics of Windsurfing*.

Exel. 2016. *Exel- Raw Materials- Reinforcementsh* [Online]. ttp://www.exelcomposites.com/en-us/english/composites/rawmaterials/reinforcements.aspx.

Fagg, S. 1997. *The development of a reversible and finitely variable camber windsurf fin*.

Gourlay, T. & Martellotta, J. 2011. *Aero-Hydrodynamics of an RS:X Olympic Racing Sailboard*.

Kunoth, A., Schlichtenmayer, M. & Schneider, C. 2007. Speed Windsurfing: Modeling and Numerics. *Int. J. Numer. Anal. Model,* 4**,** 548-558.

Miller, P. 1991. NNS composite materials properties database, unpublished composite test program report.

Shenoi, R. A. & Wellicome, J. F. 1993. *Composite Materials in Maritime Structures,* Southampton.

Sutherland, L. S. 1993. *Windsurfer Fin Hydrodynamics*, University of Southampton.

Sutherland, L. S. 2018. A review of impact testing on marine composite materials: Part I – Marine impacts on marine composites. *Compos. Struct,* (accepted for publication).

Sutherland, L. S. & Wilson, P. A. 1994. *Fin Hydrodynamics of a Windsurfer,,* Southampton.

Tsai, S. W. & Wu, E. M. 1971. A General Theory of Strength for Anisotropic Materials. *J. Compos. Mater.,* 5**,** 58-80.